2013 European Control Conference (ECC)
July 17-19, 2013, Zürich, Switzerland.

Model predictive control of a high speed switched reluctance generator system

Sava Marinkov, Bram de Jager and Maarten Steinbuch

Abstract— **This paper presents a novel voltage control strategy for the high-speed operation of a Switched Reluctance Generator. It uses a linear Model Predictive Control law based on the average system model. The controller computes the DC-link current needed to achieve the tracking of a desired voltage reference in the presence of an unknown electrical load current. Its output is converted into a pair of excitation angles (turn-on/turn-off) by means of optimized scaling and mapping, while minimizing the dominant high-speed power loss. The constraints on the average DC-link voltage and current signals are directly handled. A numerical example is provided to validate the effectiveness and the robustness of the proposed control scheme.**

I. INTRODUCTION

The Switched Reluctance Generator (SRG) has gained significant attention among researchers for purposes of high-speed electricity generation [1]–[3] due to its high reliability, fault tolerance, high power densities and the ability to operate in harsh environments. The SRG is characterized by salient poles both on the stator and the rotor and by the windings which consist exclusively of coils wound around the stator poles. The absence of brushes, rotor windings and permanent magnets helps to simplify its design and reduce manufacturing costs. It also yields a machine with a simple and rugged structure that is easy to cool and maintain and that has a wide speed range capability. These features put the SRG in a favorable position for industrial applications within, *e.g.,* automotive and aerospace industries.

However, commonly reported disadvantages of the SRG are the need for position feedback sensors and power electronics for control, acoustic noise and the presence of current/torque ripple. Its dynamics is nonlinear as it operates on a principle of changing flux which is nonlinearly dependent on both the phase current and rotor position [4].

At high speeds, the SRG is controlled in a Single-Pulse (SP) mode, where only the turn-on and turn-off excitation angles are adjusted to keep the desired output (power, voltage, etc.) close to its reference. When compared to the actual rotor position, the excitation angles provide the information when the phase current pulses should occur. Generation is achieved if the pulses appear while phase inductance is decreasing, *i.e.,* after the rotor and stator poles have passed the alignment point [5].

Many authors have treated the topic of finding the optimal excitation angles w.r.t. a certain optimality criterion. For instance, they can be found experimentally by minimizing the RMS phase current [4], [5] or by maximizing the average output to input power ratio [1]. As a consequence, an extensive experimentation is required which becomes especially cumbersome for variable speed/voltage applications. Alternatively, the optimal excitation angles can be computed using a machine Finite Element Model (FEM). This idea is pursued in [6] where the turn-on and turn-off angles are derived from FEM data by maximizing the electro-mechanical efficiency and the average produced torque. In [7] the relationship between the optimal excitation angles and the peak phase flux linkage is established over a wide speed range of SRG operation. In [3] an online search-based algorithm is proposed to find the excitation angles that correspond to the desired DC-link current with a minimal current ripple. However the need for the additional current measurement and the quality of the same, as well as the inherent sensitivity of the design on the changes in speed, limit its application.

Irrespective of the choice of optimality criterion, the general SRG control structure consists of a PI controller and a component which computes the optimal excitation angles from the PI output [4]–[7]. Typically saturation blocks are used to constrain the angles, *e.g.,* in [3], whereas the bounds on the related voltage and current signals are not addressed. Recently several papers described the use of Model Predictive Control (MPC) for the Switched Reluctance Motor (SRM) torque control [8]–[10]. One of the main advantages of using MPC over conventional control techniques such as PID is the possibility to enforce the current and voltage limits [11]. Yet, to the best of authors' knowledge there is a lack of literature concerning the use of MPC in the context of SRG control.

In this paper, the MPC is employed to control the output (DC-link, capacitor) voltage of a high-speed SRG electricity generation system and to directly handle the system input and output constraints. Specifically, the two phase 4/2 SRG of Fig. 1 is considered. The key idea exploited, which enables

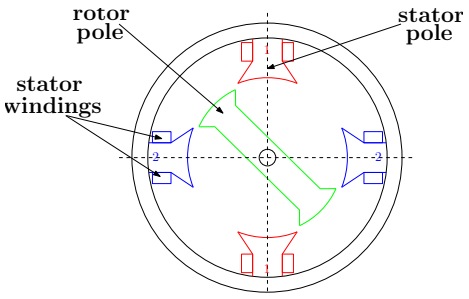

Fig. 1. Cross section of a two phase 4/2 SRG

the formulation of a linear MPC, is to observe the SRG simply as a source of charging current for the capacitor that couples the generator to the load. Namely, the MPC is designed by focusing on the dynamics of the capacitor, instead of the nonlinear SRG dynamics. Thus, it is possible to construct a computationally cheap explicit MPC law using

Sava Marinkov, Bram de Jager and Maarten Steinbuch are with the Department of Mechanical Engineering, Eindhoven University of Technology, P.O. Box 513, 5600 MB Eindhoven, The Netherlands. Email: {S.Marinkov,A.G.de.Jager,M.Steinbuch}@tue.nl

the Multi-Parametric Toolbox [12]. The MPC calculates the average DC-link current needed to track the desired capacitor voltage reference in the presence of load disturbances and signal constraints. The appropriate pair of excitation angles is further obtained from the MPC output such that the required current is generated with a reduced high-speed power loss. The paper provides a detailed description of the model-based optimization process involving the construction of the scaling and mapping between the average DC-link current and the excitation angles. The solution effectively provides the compensation for the varying speed and frees the user from the exhaustive experimentation and/or FEM modeling. However, some measurements are needed beforehand to fit the model parameters, such as the characteristic inductance values.

This paper is organized as follows. Section II provides the nonlinear continuous time equations describing the physical behavior of the SRG electrical generation system. It also introduces a simplified, high-speed model of the system used in the design of the proposed control law. In Section III the MPC voltage controller and the procedure for finding the optimized excitation angles are given. Section IV contains a representative numerical example, and conclusions are presented in Section V.

II. MODELING OF THE SRG

A. Physical model of the SRG system

The voltage equation for each SRG phase $p \in \{1,2\}$ is given by

$$\frac{\mathrm{d}\psi_p(i_p,\theta_p)}{\mathrm{d}t} = v_p - R_p i_p, \tag{1}$$

with

$$\psi_p(i_p,\theta_p) = L_p(i_p,\theta_p) i_p. \tag{2}$$

Here $i_p, v_p, \theta_p, L_p, \psi_p$ and R_p are used to denote the phase current, voltage, rotor position, inductance, flux linkage and winding resistance. Phase voltage is typically regulated by means of an Asymmetric Half Bridge Converter with two controllable switches ($S_{1,p}$ and $S_{2,p}$) per phase, as shown in Fig. 2. In Single-Pulse mode $S_{1,p}$ and $S_{2,p}$ are operated in unison: during excitation both of them are closed, resulting in $v_p = v_{dc}$, whereas during generation both are open and thus $v_p = -v_{dc}$, where v_{dc} is used to denote the capacitor voltage. Switching occurs at precise rotor locations according to the commutation rule defined by a pair of excitation angles: turn-on (θ_{on}) and turn-off (θ_{off}) angle. Thus, the excitation angles are treated as the main control inputs in the SRG electrical generation system. To capture the effect of commutation on phase voltage, it is useful to define the phase variable u_p

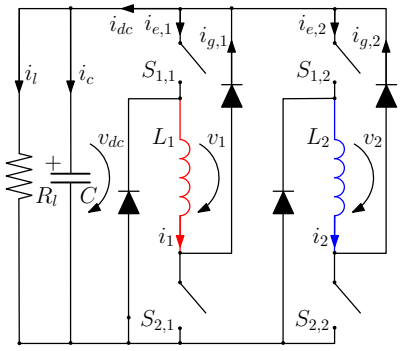

Fig. 2. Converter power circuit for a two-phase SRG.

$$u_p = \begin{cases} 1 & \text{for } \theta_{on} \le \theta_p < \theta_{off} \\ -1 & \text{for } \theta_{off} \le \theta_p < \theta_e \\ 0 & \text{otherwise,} \end{cases} \tag{3}$$

where $u_p = 1$ denotes the excitation interval, $u_p = -1$ the generation interval when $i_p \neq 0$, and $u_p = 0$ the generation intervals when $i_p = 0$. The position of the rotor during the generation interval in the moment when the phase current extinguishes is denoted with θ_e. Now, it holds

$$v_p = v_{dc} u_p. \tag{4}$$

The excitation ($i_{e,p}$) and generation ($i_{g,p}$) currents [13] are

$$i_{e,p} = \begin{cases} i_p & \text{for } u_p = 1, \\ 0 & \text{otherwise,} \end{cases} \tag{5}$$

$$i_{g,p} = \begin{cases} i_p & \text{for } u_p = -1, \\ 0 & \text{otherwise,} \end{cases} \tag{6}$$

and the cumulative DC-link current is

$$i_{dc} = \sum_{p=1}^{m} i_{g,p} - \sum_{p=1}^{m} i_{e,p}, \tag{7}$$

where $m = 2$ is the total phase count. The last equation can be rewritten in a more compact form as

$$i_{dc} = -\sum_{p=1}^{m} i_p u_p. \tag{8}$$

Furthermore, the change in the capacitor voltage is a consequence of the difference between the DC-link current and the electrical load current i_l, *i.e.,*

$$\frac{\mathrm{d}v_{dc}}{\mathrm{d}t} = \frac{1}{C}(i_{dc} - i_l) \tag{9}$$

where C is the DC-link capacitance.

Finally, the phase rotor position θ_p, for $p \in \{1,2\}$ is given by

$$\frac{\mathrm{d}\theta}{\mathrm{d}t} = \omega, \tag{10}$$

$$\theta_p = \theta + (p-1)\pi/2 \pmod{\pi}, \tag{11}$$

where ω and θ represent the angular rotor speed and position. Note that the unaligned rotor position w.r.t. the first phase corresponds to the situation when $\theta = \theta_{p=1} = 0$.

B. Model of the SRG system for control

The full SRG system model is characterized by its inherent nonlinearity, presence of integer variables and due to high-speed application, also fast dynamics. These properties pose significant challenges and limit the usage of such a model for the design and real-time implementation of model-based control. For these reasons, a model for control is derived by averaging the full SRG system dynamics given by (1)-(11) during one period of phase current $T = \pi/\omega$ (half of one full rotation).

When the SRG operates above base speed [4] it is reasonable to consider that the phase inductance is independent of phase current, *i.e.,* $L_p(i_p,\theta_p) = L_p(\theta_p)$ [14]. As high rotational speeds imply short phase current build-up times, the resulting peak currents will remain low and thus

have a negligible saturation effect on the magnetic material. Here, the phase inductance is modeled as a piecewise affine function of rotor position [15] as shown in Fig. 3, where

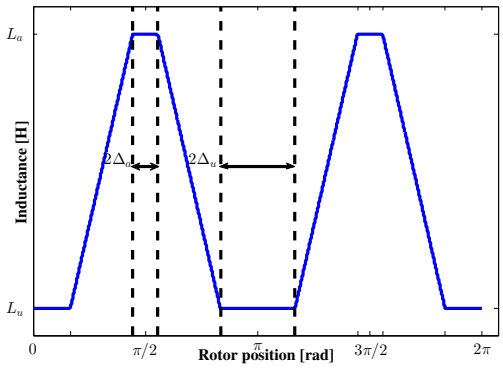

Fig. 3. Piecewise affine inductance profile

L_a and L_u, and Δ_a and Δ_u are used to denote the aligned and unaligned inductance, and half of the alignment and unalignment angles. Therefore, it holds

$$i_p(\theta_p) = \frac{\psi_p(i_p,\theta_p)}{L_p(\theta_p)}. \tag{12}$$

By ignoring the phase ohmic voltage drop $R_p i_p$ in (1), as it is typically very small when compared to v_p, a simplified expression [16] for flux linkage is obtained

$$\psi_p(i_p,\theta_p) = \int_0^t v_p(\tau)\,\mathrm{d}\tau, \tag{13}$$

for $kT \le t \le (k+1)T$, $k \in \mathbb{N}_0$. Assuming that v_{dc} is approximately equal to the average capacitor voltage V_{dc} and that the rotor speed changes on a far bigger timescale then T, *i.e.,* $\omega(t)$ is approximately constant, during T, it further holds

$$\psi_p(i_p,\theta_p) = \frac{V_{dc}}{\omega}\int_0^{\theta_p} u_p(\alpha)\,\mathrm{d}\alpha = \frac{V_{dc}}{\omega}\psi_p^*(i_p,\theta_p). \tag{14}$$

Given the definition of u_p, it is straightforward to compute that the integral ψ_p^* in the last expression (and thus also ψ_p and i_p) becomes zero at the angle

$$\theta_e = \theta_{off} + (\theta_{off} - \theta_{on}). \tag{15}$$

By inserting (12) into (8) and calculating the mean of the result over one half of rotation, we obtain the average DC-link current

$$I_{dc} = -\frac{V_{dc}}{\omega}\frac{m}{\pi}\int_0^{\pi}\frac{\psi_p^*(i_p,\theta_p)u_p(\theta_p)}{L_p(\theta_p)}\,\mathrm{d}\theta. \tag{16}$$

Expression (16) can be further simplified analytically since both the flux linkage and inductance are piecewise affine, and phase input u_p is piecewise constant. Therefore, it holds

$$I_{dc} = -\frac{V_{dc}}{\omega}\frac{m}{\pi}\sum_{n=1}^{N}\int_{g_n}^{G_n}\frac{a_n\theta + b_n}{c_n\theta + d_n}\,\mathrm{d}\theta, \tag{17}$$

where a_n and b_n are the slope and the offset of $\psi_p^* u_p$, and c_n and d_n are the slope and the offset of L_p, in the interval $[g_n, G_n]$. The interval bounds g_n and G_n are selected from a set $\left[\{0,\Delta_u,\frac{\pi}{2}\pm\Delta_a,\pi-\Delta_u,\pi\}\cup\{\theta_{on},\theta_{off},\theta_e\}\mathrm{mod}\ \pi\right]$ in such a way that the resulting intervals are mutually disjunct. Define

$$W_n = \left[\frac{a_n\theta}{c_n} - \frac{\ln(d_n + c_n\theta)\,(a_n d_n - b_n c_n)}{{c_n}^2}\right]\Big|_{g_n}^{G_n}, \tag{18}$$

$$R_n = \left[\frac{\theta\,(2b_n + a_n\theta)}{2d_n}\right]\Big|_{g_n}^{G_n}, \tag{19}$$

then the solution for the average DC-link current reads

$$I_{dc} = -\frac{V_{dc}}{\omega}\frac{m}{\pi}\left[\sum_{n,c_n\neq 0} W_n + \sum_{n,c_n=0} R_n\right]. \tag{20}$$

Finally, averaging (9) yields:

$$\frac{\mathrm{d}V_{dc}}{\mathrm{d}t} = \frac{1}{C}(I_{dc} - I_l), \tag{21}$$

where I_l denotes the average load current flowing through the resistor R_l.

III. CONTROL OF THE SRG

The proposed control structure is illustrated in Fig. 4.

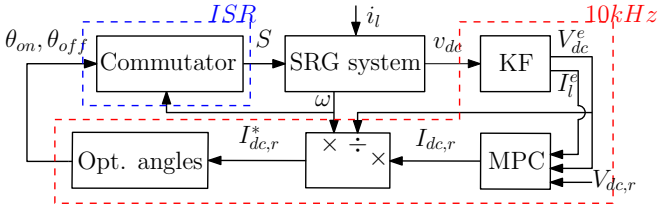

Fig. 4. Block diagram of the SRG control system

Using the linear DC-link capacitor model (21) MPC calculates the value $I_{dc,r}$ of the DC-link current I_{dc} necessary to make V_{dc}^e follow the reference $V_{dc,r}$ in the presence of load current disturbance I_l^e, where V_{dc}^e and I_l^e are respectively the Kalman filter KF estimates of V_{dc} and I_l. At the same time, MPC ensures that both $I_{dc,r}$ and V_{dc}^e lie within the pre-specified bounds. The computed MPC output $I_{dc,r}$ is translated into a $\{\theta_{on},\theta_{off}\}$ pair by means of scaling and mapping. Scaling is performed first, w.r.t. the ω/V_{dc} ratio. The scaling result $I_{dc,r}^*$ is mapped to the excitation angles through a map derived via an off-line optimization procedure based on (20) and aiming for the reduction of the SRG high-speed power loss. Finally, a commutator block is used to convert the excitation angles into the switching signals S that drive the commutation of the machine phases.

A. Model Predictive Voltage Control

Due to a time-discrete character of model predictive control, we start by discretizing (using zero-order hold) the average capacitor voltage dynamics. Defining the state $x(k)$, input $u(k)$ and the output $y(k)$ as

$$\begin{aligned} x(k) &= \begin{bmatrix} V_{dc}^e(k) & I_l^e(k) \end{bmatrix}^T, \\ u(k) &= I_{dc,r}(k), \\ y(k) &= V_{dc}^e(k), \end{aligned} \tag{22}$$

the following time-discrete state-space representation of (21) is obtained:

$$\begin{aligned} x(k+1) &= \underbrace{\begin{bmatrix} 1 & \frac{-T}{C} \\ 0 & 1 \end{bmatrix}}_{A} x(k) + \underbrace{\begin{bmatrix} \frac{T}{C} \\ 0 \end{bmatrix}}_{B} u(k) + \rho(k), \quad (23) \\ y(k) &= \underbrace{\begin{bmatrix} 1 & 0 \end{bmatrix}}_{C} x(k) + \eta(k). \end{aligned}$$

With $\rho(k) \in \mathbb{R}^2$ and $\eta(k) \in \mathbb{R}$ we denote the zero-mean white state and measurement noise, defined by the following noise covariance data: $W_1 = E(\rho\rho^T)$ and $W_2 = E(\eta\eta^T)$. Here, $E(\bullet)$ represents the expected value. Since the system is observable, a standard Kalman filter can be designed to estimate the state x. For brevity we skip the filter implementation details and refer the reader to, *e.g.,* [17].

Note that the model (23) includes the load current disturbance as a part of the state. The idea stems from the Internal Model Principle (IMC) [18], while the model choice represents a commonly used strategy in MPC [19] used to remove the possibility of steady-state offset due to constant or nonzero mean disturbances.

By representing the predicted state and the output at time $k+j$, given the state and the output at time k, as $x_{k+j|k}$ and $y_{k+j|k}$, we proceed to define the MPC problem at time k:

$$\begin{aligned} \min_{U \triangleq u(k),\ldots,u(k+N-1)} \quad & J(U, x(k)) = x_{k+N|k} P_N x_{k+N|k} + \quad (24) \\ & \sum_{j=0}^{N-1} [R u_{k+j}^2 + Q_y (y_{k+j|k} - r_{k+j|k})^2 \\ & + x_{k+j|k}^T Q x_{k+j|k}] \\ \text{subj. to} \quad & \\ & x_{k|k} = x(k) \\ & x_{k+j+1|k} = A x_{k+j|k} + B u_{k+j}, j \geq 0 \\ & 0 \leq u_{k+j} \leq u_{max}, j = 0 \ldots N-1, \\ & \Delta u_{min} \leq \Delta u_{k+j} \leq \Delta u_{max}, j = 0 \ldots N-1, \\ & y_{min} \leq y_{k+j} \leq y_{max}, j = 1 \ldots N-1, \end{aligned}$$

where N denotes the prediction horizon, Q a weighting matrix on the states, R a weighting on the input, Q_y a weighting on the output, P_N a weight on the terminal state, u_{max} the maximum allowed average DC-link current, $\Delta u_{min}, \Delta u_{max}$ minimum and maximum allowed slew rate of the average DC-link current, y_{min}, y_{max} are limits on the average DC-link voltage and $\Delta u_k = u_k - u_{k-1}$ is the incremental input.

The standard MPC receding horizon strategy implies that the optimization of the performance index J is performed online at each time moment k. Afterwards, only the first entry of the optimal input vector U is applied to the system. However, in [20] a different MPC approach is presented which is used here as well. It is shown that the MPC problems such as (24) can be rewritten in the form of a multi-parametric Quadratic Program (mp-QP) that can be solved off-line. The result is an explicit MPC controller – a piecewise-affine continuous-state feedback defined on a finite number of contiguous regions of the state-space:

$$u_j(k) = F_j x(k) + G_j, \quad (25)$$

where j represents the active region index and F_j and G_j are the outcome of the related optimization procedure. Online computation of the control input $u(k)$ reduces to an active region search and a subsequent simple linear function evaluation. In this work we have used the *multiparametric toolbox* (MPT) [12] for Matlab to compute the explicit MPC controller for tracking of the varying voltage reference. The toolbox provides the solver and the routines for the region partitioning and the active region search, suitable for both simulation and implementation [11]. For reference tracking the toolbox internally extends the state vector x with the reference r and reformulates the dynamics (and the problem) in Δu form. This yields the following state equation:

$$\begin{bmatrix} x(k+1) \\ u(k) \\ r(k+1) \end{bmatrix} = \begin{bmatrix} A & B & 0 \\ 0 & 1 & 0 \\ 0 & 0 & 1 \end{bmatrix} \begin{bmatrix} x(k) \\ u(k-1) \\ r(k) \end{bmatrix} + \begin{bmatrix} B \\ 1 \\ 0 \end{bmatrix} \Delta u(k). \quad (26)$$

B. Optimized Excitation Angles

Through the phase input, I_{dc} depends on both the turn-on and turn-off angle (16). This creates space for the definition of an additional criterion to be minimized for each average DC-link current $I_{dc,r}$ requested by the MPC, yielding the "optimized excitation angles." We select a performance function related to the energy lost in the SRG during high-speed operation.

Overall the main losses in the SRG are the copper and the iron (core) losses, P_{Cu} and P_{Fe}. The accurate estimation of P_{Cu} is hindered by the fact that it is proportional to the square of the non-sinusoidal, RMS phase current. However, it has been shown that at high speeds the importance of P_{Cu} decreases and P_{Fe} becomes the dominant loss component [21]. The iron loss is often separated into the losses due to hysteresis P_{hy} and eddy currents P_{ed} in the iron material [22] approximated by:

$$\begin{aligned} P_{hy} &= k_1 f \psi^{k_2}, \quad (27) \\ P_{ed} &= k_3 f^2 \psi, \end{aligned}$$

where f is the excitation frequency of the flux linkage and k_1, k_2 and k_3 are some empirical constants. From (27) it follows that the iron loss can be reduced by minimizing the flux linkage ψ. Thus, using (14) the peak phase flux linkage ψ_{max} and the average flux linkage Ψ during period T are derived:

$$\begin{aligned} \psi_{max} &= \frac{V_{dc}}{\omega}(\theta_{off} - \theta_{on}), \quad (28) \\ \Psi &= \frac{V_{dc}}{\omega}\frac{m}{\pi}(\theta_{off} - \theta_{on})^2. \end{aligned}$$

The performance function G is then selected as

$$G = (\theta_{off} - \theta_{on})^2, \quad (29)$$

since the minimization of G will result in minimization of both ψ_{max} and Ψ and, in the context of a high-speed SRG application, also the dominant, iron loss.

Finally, the "optimized excitation angles" are defined as a solution of the following nonlinear programming problem

$$\begin{aligned} \min_{\theta_{on}, \theta_{off}} \quad & (\theta_{off} - \theta_{on})^2, \quad (30) \\ \text{s.t.} \quad & \theta_{on} \leq \theta_{off}, \\ & I_{dc}^*(\theta_{on}, \theta_{off}) = I_{dc,r}^*, \end{aligned}$$

where $I_{dc}^* = I_{dc}\omega / V_{dc}$ and $I_{dc,r}^* = I_{dc,r}\omega / V_{dc}$ are the scaled average and the reference average DC-link current. Motivated

by (16), scaling removes ω and V_{dc} from (30) and effectively compensates for the influence of the (ω, V_{dc}) operating point on the SRG operation.

IV. NUMERICAL EXAMPLE

The parameter values used to specify an example 4/2 SRG system, related signal bounds, Kalman filter and the explicit MPC controller, are given in Table I. The voltage tracking controller is designed according to the procedure described in Section III-A, resulting in a PWA control law defined over 101 regions in 4 state dimensions. Fig. 5 shows the projection of the region partition of the controller on the first three state variables of the augmented system given by (26).

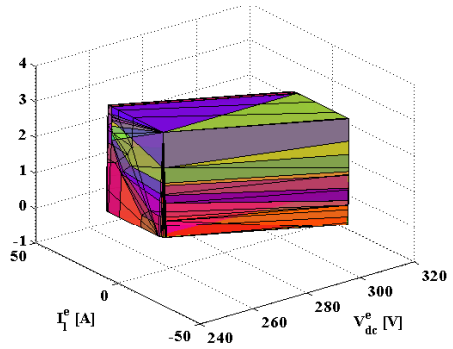

Fig. 5. The projection of the region partition of the controller on the first three state variables: estimated average capacitor voltage, estimated average load current and average reference DC-link current

TABLE I
PARAMETER VALUES

Machine (design)	MPC
$L_a = 5.5$ mH	$P_N = 0$
$L_u = 0.5$ mH	$R = 80$
$\Delta_a = 10^\circ$	$Q_y = 1$
$\Delta_u = 30^\circ$	$Q = [1 \quad 0; \quad 0 \quad 0]$
$C = 250\ \mu$F	$N = 5$
$\omega_{max} = 100$ krpm	$T = 0.1$ ms
Signal bounds	**Kalman filter**
$u \in [0, 3]$ A	$W_1 = [1 \quad 0; 0 \quad 1]$
$\Delta u \in [-1, 1]$ A	$W_2 = 50000$
$y \in [255, 305]$ V	

A contour plot of the optimization problem (30) is shown in Fig. 6. The optimization is performed for each value $I^*_{dc,r}$ in a range $[0, \frac{\omega_{max} u_{max}}{y_{min}}]$. Then, the obtained optimized excitation angle data is fitted (Fig. 7) for purposes of accurate online lookup by means of suitable functions:

$$\begin{aligned} \theta_{on}^{opt}(I^*_{dc,r}) &= c_1 (I^*_{dc,r})^{c_2} + c_3, \\ \theta_{off}^{opt}(I^*_{dc,r}) &= c_3, \end{aligned} \tag{31}$$

where $[c_1 \ldots c_3] = [-0.068 \quad 0.435 \quad 2.597]$.

Simulation of the proposed controller (Fig. 8) shows that V_{dc} (blue) tracks the reference $V_{dc,r}$ (green) while speed (Fig. 9) and the load current (Fig. 10) are varying. From the initial 260 V, V_{dc} reaches the desired set-point of 280 V within 0.02 s. At $t_1 = 0.1$ s, I_l drops from 0.93 A to 0.46 A, due to the change in R_l from 300 Ω to 600 Ω (lighter load). However, the controller is able to quickly compensate for the sudden increase in the capacitor voltage. Similar but opposite situation occurs at $t_2 = 0.2$ s when a heavier load

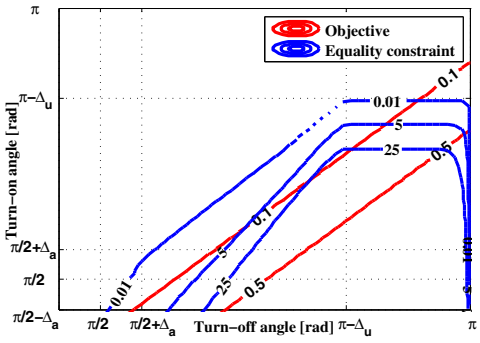

Fig. 6. Contour plot of the optimization problem

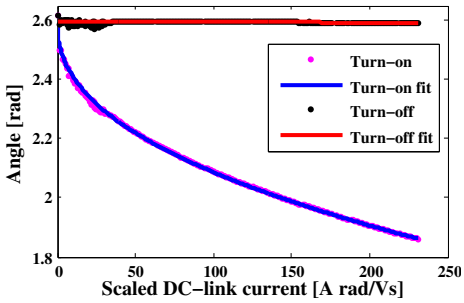

Fig. 7. Optimized excitation angles

is introduced, *i.e.,* when R_l decreases from 600 Ω to 150 Ω. Namely, the controller modifies the excitation angles (Fig. 8) to compensate for the voltage drop as I_l rises from 0.46 A to 1.86 A. The effect of step change in $V_{dc,r}$ can be seen at $t_3 = 0.3$ s. Again the requested level is quickly obtained, with a minimal overshoot. Note that the controller keeps $I_{dc,r}$ and the V_{dc} within pre-specified bounds. The occasional peaks in the true I_{dc} that extend beyond the allowable limits are attributed to the windowing inaccuracies in the Variable-Frequency Moving Average Filter (window $T = \pi/\omega$) that was used to compute it from the the instantaneous DC-link current i_{dc}. Finally, we mention that the change in speed (from 2500 to 3000 rad/s in 0.4 s) had an almost negligible effect on the overall tracking performance of the system, *i.e.,* the design is fairly robust w.r.t. the speed variation.

V. CONCLUSIONS

In this paper a new voltage control scheme for the SRG electricity generation system was proposed based on explicit MPC. The controller is designed to reduce the SRG high-speed power loss and to keep the average DC-link current and the output voltage within pre-specified bounds. Simulations have shown that the controlled system is capable of smooth voltage tracking in the presence of both varying load current and changing speed.

REFERENCES

[1] Y. Sozer and D. Torrey, "Closed Loop Control of Excitation Parameters for High Speed Switched-Reluctance Generators," *IEEE Transactions on Power Electronics*, vol. 19, no. 2, pp. 355–362, Mar. 2004.

[2] M. Michon, S. Calverley, and K. Atallah, "Operating strategies for switched reluctance generators in exhaust gas energy recovery systems," in *2011 IEEE International Electric Machines & Drives Conference (IEMDC)*. IEEE, May 2011, pp. 1609–1614.

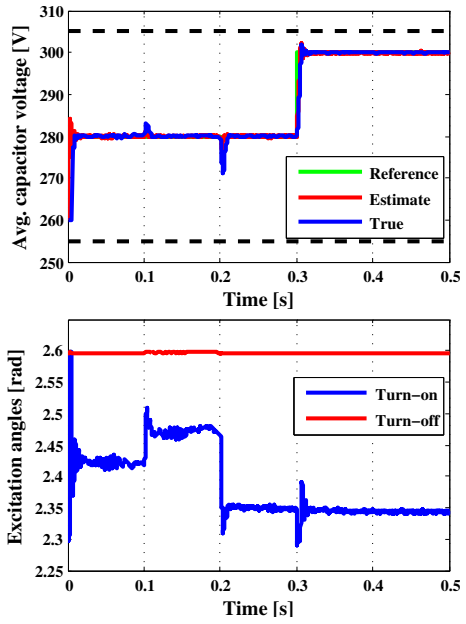

Fig. 8. Average output voltage (top) and excitation angles (bottom)

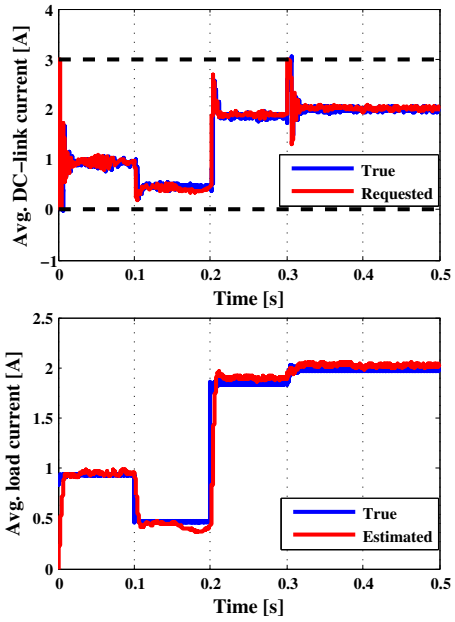

Fig. 10. Average DC-link current (top) and load current (bottom)

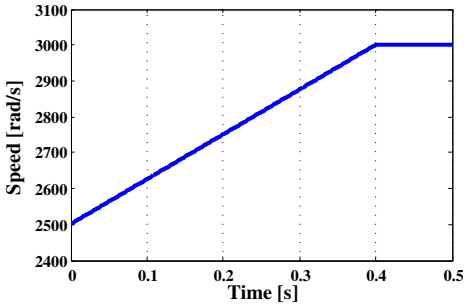

Fig. 9. Rotor speed

[3] S. Narla, Y. Sozer, and I. Husain, "Switched reluctance generator controls for optimal power generation and battery charging," in *2011 IEEE Energy Conversion Congress and Exposition*. IEEE, Sep. 2011, pp. 3575–3581.

[4] D. Torrey, "Switched reluctance generators and their control," *IEEE Transactions on Industrial Electronics*, vol. 49, no. 1, pp. 3–14, Feb. 2002.

[5] E. Kennedy, A. Murphy, M. Condon, and J. Dowling, "Closed-loop control of switched reluctance generators," *COMPEL: The International Journal for Computation and Mathematics in Electrical and Electronic Engineering*, vol. 24, no. 2, pp. 662–681, 2005.

[6] C. S. Dragu and R. J. M. Belmans, "Optimal Firing Angles Control for Four-Quadrant Operation of an 8/6 SRM," in *Proceedings of 10th European Conference on Power Electronics and Applications*, Toulouse, 2003, pp. 1–10.

[7] C. Mademlis and I. Kioskeridis, "Optimizing Performance in Current-Controlled Switched Reluctance Generators," *IEEE Transactions on Energy Conversion*, vol. 20, no. 3, pp. 556–565, Sep. 2005.

[8] A. Sadeghzadeh and B. Araabi, "Auto-tune Predictive Control of Switched Reluctance Motor," in *2006 IEEE International Symposium on Industrial Electronics*. IEEE, Jul. 2006, pp. 335–340.

[9] H. Peyrl, G. Papafotiou, and M. Morari, "Model predictive torque control of a Switched Reluctance Motor," in *2009 IEEE International Conference on Industrial Technology*. IEEE, Feb. 2009, pp. 1–6.

[10] J. Villegas, S. Vazquez, J. Carrasco, and I. Gil, "Model predictive control of a switched reluctance machine using discrete space vector modulation," in *2010 IEEE International Symposium on Industrial Electronics*. IEEE, Jul. 2010, pp. 3139–3144.

[11] S. Bolognani, L. Peretti, and M. Zigliotto, "Design and Implementation of Model Predictive Control for Electrical Motor Drives," *IEEE Transactions on Industrial Electronics*, vol. 56, no. 6, pp. 1925–1936, Jun. 2009.

[12] M. Kvasnica, P. Grieder, M. Baotić, and M. Morari, "Multi-Parametric Toolbox (MPT)," in *Hybrid Systems: Computation and Control*, R. Alur and G. Pappas, Eds. Springer Berlin / Heidelberg, 2004, pp. 121–124.

[13] V. Hrabovcova, P. Rafajdus, and M. Liptak, "Output Power of Switched Reluctance Generator With Regard To the Phase Number and Number of Stator and Rotor Poles," *Electronics and Electrical Engineering*, vol. 109, no. 3, Mar. 2011.

[14] K. Vijayakumar, R. Karthikeyan, S. Paramasivam, R. Arumugam, and K. Srinivas, "Switched Reluctance Motor Modeling, Design, Simulation, and Analysis: A Comprehensive Review," *IEEE Transactions on Magnetics*, vol. 44, no. 12, pp. 4605–4617, Dec. 2008.

[15] I. Kioskeridis and C. Mademlis, "Optimal Efficiency Control of Switched Reluctance Generators," *IEEE Transactions on Power Electronics*, vol. 21, no. 4, pp. 1062–1072, Jul. 2006.

[16] P. Asadi, M. Ehsani, and B. Fahimi, "Design and Control Characterization of Switched Reluctance Generator for Maximum Output Power," in *Twenty-First Annual IEEE Applied Power Electronics Conference and Exposition*. IEEE, Mar. 2006, pp. 1639–1644.

[17] M. S. Grewal and A. P. Andrews, *Kalman Filtering: Theory and Practice*. Prentice Hall, 1993.

[18] B. Francis and W. Wonham, "The internal model principle of control theory," *Automatica*, vol. 12, no. 5, pp. 457–465, Sep. 1976.

[19] G. Pannocchia and J. B. Rawlings, "Disturbance models for offset-free model-predictive control," *AIChE Journal*, vol. 49, no. 2, pp. 426–437, Feb. 2003.

[20] A. Bemporad, M. Morari, V. Dua, and E. Pistikopoulos, "The explicit solution of model predictive control via multiparametric quadratic programming," in *Proceedings of the 2000 American Control Conference*, vol. 2, Jun. 2000, pp. 872–876.

[21] P. Materu and R. Krishnan, "Estimation of switched reluctance motor losses," *IEEE Transactions on Industry Applications*, vol. 28, no. 3, pp. 668–679, May 1992.

[22] P. Kjaer, P. Nielsen, L. Andersen, and F. Blaabjerg, "A new energy optimizing control strategy for switched reluctance motors," *IEEE Transactions on Industry Applications*, vol. 31, no. 5, pp. 1088–1095, Sep. 1995.